Distortion correction and cross-talk compensation algorithm for use with an imaging spectrometer based spatially resolved diffuse reflectance system

Derek J. Cappon, Thomas J. Farrell, Qiyin Fang, and Joseph E. Hayward

Citation: Rev. Sci. Instrum. **87**, 123112 (2016); doi: 10.1063/1.4973122
View online: http://dx.doi.org/10.1063/1.4973122
View Table of Contents: http://aip.scitation.org/toc/rsi/87/12
Published by the American Institute of Physics

Distortion correction and cross-talk compensation algorithm for use with an imaging spectrometer based spatially resolved diffuse reflectance system

Derek J. Cappon,[1] Thomas J. Farrell,[1] Qiyin Fang,[2,3] and Joseph E. Hayward[1,2]
[1]*Radiation Sciences Graduate Program, McMaster University, 1280 Main St. W, Hamilton, Ontario L8S 4K1, Canada*
[2]*Department of Engineering Physics, McMaster University, 1280 Main St. W, Hamilton, Ontario L8S 4L7, Canada*
[3]*School of Biomedical Engineering, McMaster University, 1280 Main St. W, Hamilton, Ontario L8S 4L7, Canada*

(Received 4 August 2016; accepted 12 December 2016; published online 28 December 2016)

Optical spectroscopy of human tissue has been widely applied within the field of biomedical optics to allow rapid, *in vivo* characterization and analysis of the tissue. When designing an instrument of this type, an imaging spectrometer is often employed to allow for simultaneous analysis of distinct signals. This is especially important when performing spatially resolved diffuse reflectance spectroscopy. In this article, an algorithm is presented that allows for the automated processing of 2-dimensional images acquired from an imaging spectrometer. The algorithm automatically defines distinct spectrometer tracks and adaptively compensates for distortion introduced by optical components in the imaging chain. Crosstalk resulting from the overlap of adjacent spectrometer tracks in the image is detected and subtracted from each signal. The algorithm's performance is demonstrated in the processing of spatially resolved diffuse reflectance spectra recovered from an Intralipid and ink liquid phantom and is shown to increase the range of wavelengths over which usable data can be recovered. *Published by AIP Publishing.* [http://dx.doi.org/10.1063/1.4973122]

I. INTRODUCTION

Imaging spectrometers are used in various scientific applications in order to analyze a signal in both the spectral and spatial domains. Imaging spectrometers have been utilized for large scale hyperspectral imaging with both terrestrial[1] and astronomical[2] applications and smaller scale biomedical applications including hyperspectral microscopy,[3] fluorescence,[4] and reflectance[5] spectroscopy. In this paper, a processing algorithm is presented that corrects for distortion and crosstalk effects in images obtained from a fibre optic probe coupled to an imaging spectrometer.

Diffuse reflectance spectroscopy (DRS) is an optical technique commonly used to analyze the composition of human tissue. It has been investigated for use in many different applications of biomedical optics, from the characterization of skin lesions[6] to discrimination of esophageal malignancies[7] to the *in vivo* assessment of colon tissue in colorectal cancer patients.[8] A broadband light source (ultraviolet, visible, or near infrared depending on the application) illuminates the tissue, and a spectrometer is used to collect the reflectance spectrum allowing for quantitative analysis of the results.[9–11] Optical fibres are often used both to deliver light to the tissue and collect the resulting reflectance. The features of the reflectance spectrum can be observed directly to analyze tissue composition,[12,13] or used to recover the optical properties of the sample, providing a quantified measure of how light interacts with the tissue.[8,14,15] Optical properties recovered from diffuse reflectance data include the reduced scattering coefficient (μ_s') and the absorption coefficient (μ_a).

Methods for recovering optical properties from diffuse reflectance data include frequency (or time) domain analysis[16,17] and spatial domain analysis.[8,15] In either of these approaches, measured reflectance curves are fit with the results of a theoretical model generated from approximate solutions of the diffusion equation or Monte Carlo simulation. The optical properties that generate the best fit to the measured data are accepted as the properties of the tissue.

A well-established method for measuring spatially resolved diffuse reflectance data uses an imaging spectrometer and CCD camera to capture the output from multiple optical fibres.[5,10,18] Detector fibres are placed at different distances from a source fibre so that the system is able to simultaneously capture both spatially and spectrally resolved data in a single measurement. The fibres are embedded in a probe, making for an easy to use measurement device with fixed source-detector distances (SDDs). At the opposite end, the fibers are connected to the imaging spectrometer and CCD. Each detector fibre is physically separated from the others at the entrance to the spectrometer, as demonstrated in Fig. 1(a). As the spectrometer resolves each fibre's output by wavelength, this produces an image of "tracks" on the CCD, Fig. 1(b). Some image processing is required to separate each track from its neighbours and determine the spectral intensity of each detector fibre.

In this article, an automatic image processing routine used to define spectrometer tracks in an imaging spectrometer based spatially resolved diffuse reflectance system is described. This is a flexible improvement over previous algorithms, as it compensates for distortion introduced by the

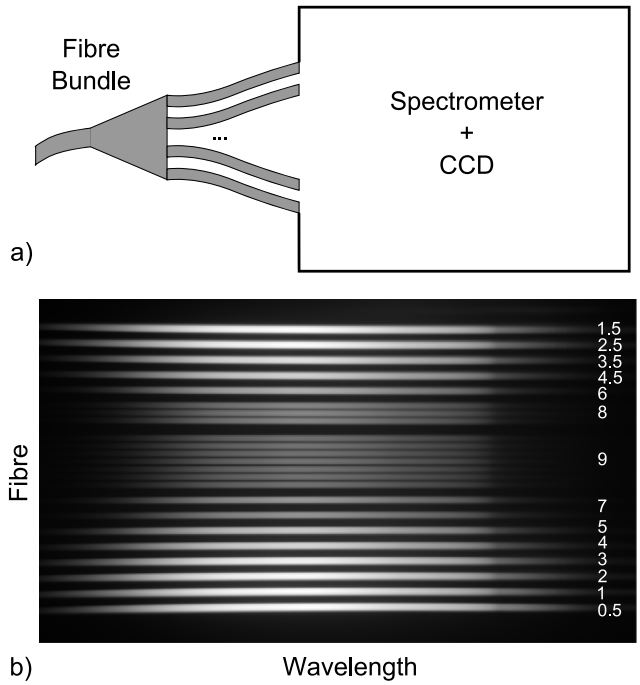

FIG. 1. (a) Individual fibres are physically separated before entering the spectrometer. (b) An example of the image acquired by the CCD. Each track corresponds to a separate fibre and the source-detector distances of each fibre are indicated in mm.

optical chain and adaptively subtracts crosstalk resulting from the overlap of detector tracks. Although this algorithm was designed specifically for the setup described below, it can be readily adapted for use with other imaging spectrometer based systems.

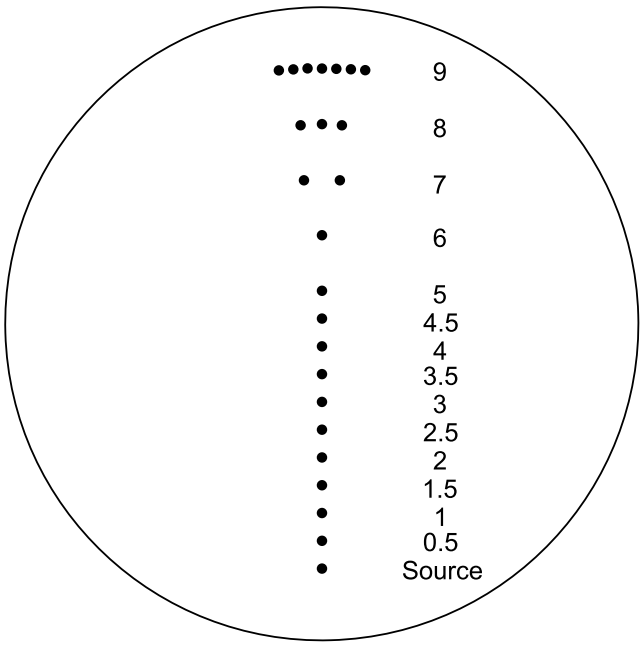

FIG. 2. The arrangement of fibres across the surface of the epoxy probe. The source fibre is used to deliver light to the tissue, and the centre to centre distance of each detector from the source is indicated in mm. Each fibre has a core diameter of 100 μm.

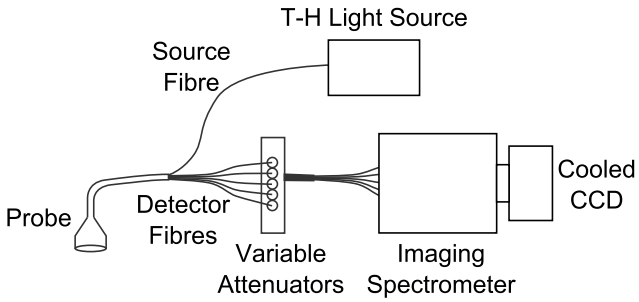

FIG. 3. The equipment used to acquire diffuse reflectance spectra.

II. MATERIALS AND METHODS

The equipment used by our group has been described previously by Pekar and Patterson.[5] In summary, a broadband tungsten-halogen light source (Oriel Instruments, Stratford, CT) was used to illuminate a sample through a 100 μm optical fibre embedded in a handheld epoxy probe. Detector fibres were arranged across the surface of this probe according to the layout shown in Fig. 2. Multiple detector fibres were used at the outermost distances to partially compensate for the decreased signal at these distances. Each detector fibre was attached to a variable attenuator (OZ optics, Ottawa, Ontario) to allow further balancing of the signals and fit the entire image within the dynamic range of the CCD. The outputs of the attenuators were sent through an imaging spectrometer (Kaiser Optical Systems, Ann Arbor, MI) and the image was acquired using an attached cooled CCD (Princeton Instruments, Trenton, NJ). The digitized signal was collected using Princeton Instrument's WinSpec software package and all analysis was performed using Matlab (The Mathworks, Natick, MA). A diagram of the system is shown in Fig. 3. For every acquisition, a dark background image was also collected and subtracted from the data.

The reflectance from each detector fibre broadens as it travels from the spectrometer grating to the CCD such that the signal from two separate fibres overlaps slightly. This undesired effect is referred to as crosstalk in this article. Despite the use of variable attenuators on each fibre, the signals from fibres at shorter SDDs were still more intense than those at

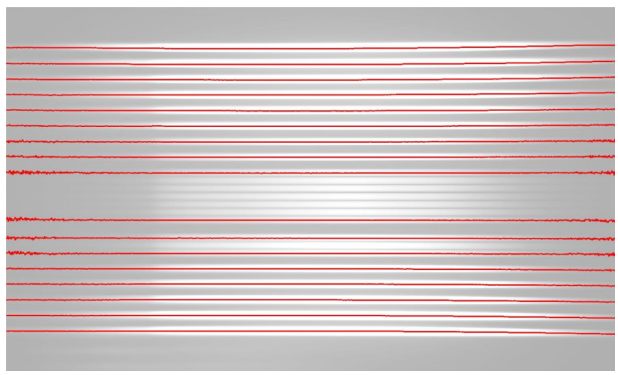

FIG. 4. The curvature of the tracks on the spectrometer image. The locations of peak intensity of selected tracks are plotted in red. Examination of the tracks reveals a distinct curvature towards the top and bottom of the image, most significant for the outermost tracks.

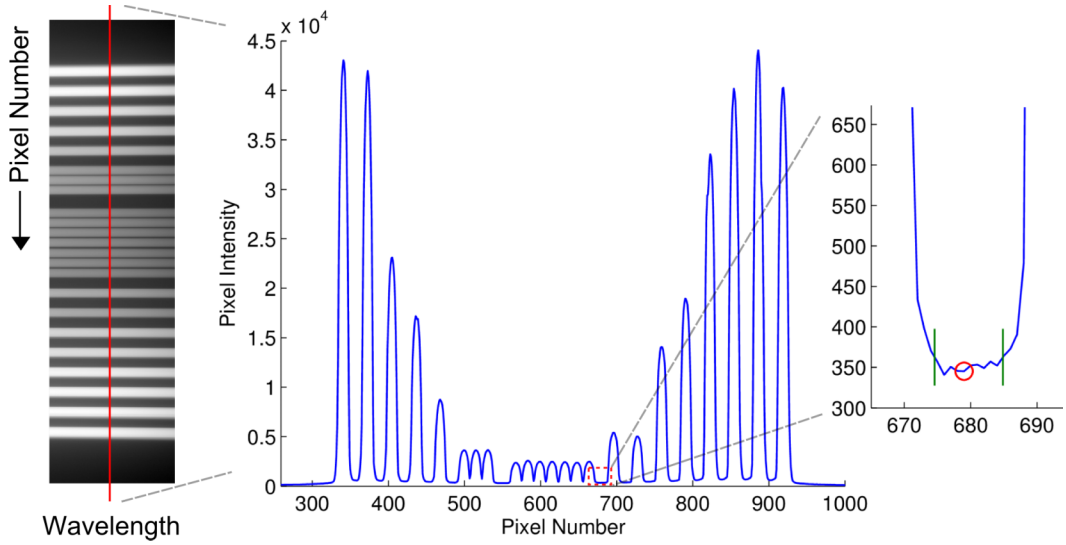

FIG. 5. Track edge identification. This step in the algorithm operates along vertical lines through the image, with each line having a width of 1 pixel, approximately 0.5 nm. The plot displays the image intensity along the 650 nm line. Inset: the midpoint between two adjacent tracks is identified by finding the local minimum of smoothed data in this region. The red circle identifies the point in the original (unsmoothed) data that corresponds to the minimum of the smoothed data. The edges of the two adjacent tracks are defined as the points at which the intensity is 1.05 times the intensity at the circled point (the two lines at 675 and 685).

larger distances. To reduce the influence of crosstalk in the final image, the fibres were arranged such that those with a more intense signal (shorter SDDs) were located at the top and bottom of the image, while the less intense signals (large SDDs) were clustered near the middle. The positioning of each fibre on the CCD image is shown in Fig. 1(b).

Inspection of the CCD images reveals that each track follows a curved shape. This is demonstrated in Fig. 4, a plot of the peak intensity of selected tracks across the spectrum. The curvature is more pronounced for the outermost tracks and results from image distortion between the spectrometer and CCD. To compensate for this distortion and other potential irregularities in track size, an algorithm was developed to automatically define track boundaries. Although these boundaries are not expected to vary significantly for different measurements, the algorithm is applied to CCD images on an individual basis.

The initial steps in the analysis were applied at each wavelength along lines perpendicular to the intensity tracks, as demonstrated in Fig. 5. To find the midpoint between each track, data in this region were first smoothed using the Matlab Curve Fitting Toolbox "smooth" function with the "loess" option. The midpoint was then identified by finding the local minimum (zero crossing of the first derivative) in the smoothed data. The edges of each adjacent track were then defined as the points where the (unsmoothed) data crossed a threshold of 1.05 times the pixel value at the midpoint. A threshold of 5% was chosen as it was observed to be consistently above the noise level of the data in a large training set. This process is illustrated in Fig. 5.

Because the algorithm depended on the data reaching a local minimum, it could not be used to find the top and bottom edges of the two outermost tracks. Instead, the outermost boundaries of these tracks were estimated at selected wavelengths in a series of training images and averaged to provide an estimate of the track boundaries across the spectrum. Data were smoothed by fitting each track boundary with a two term

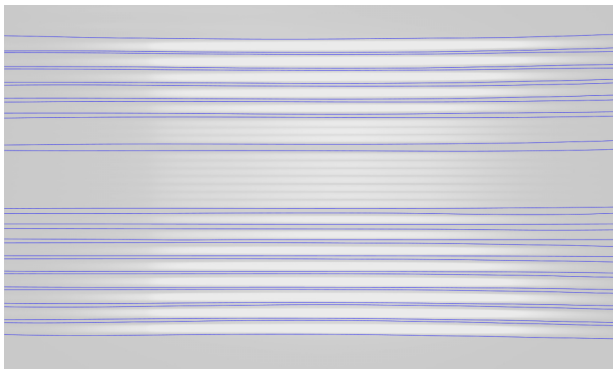

FIG. 6. Final track boundaries. The raw output of the algorithm was smoothed by fitting with the Gaussian function of Eq. (1).

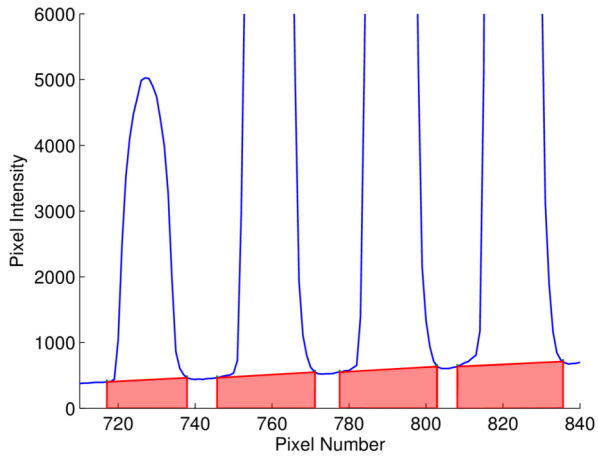

FIG. 7. Crosstalk subtraction. The algorithm identified the highlighted areas as crosstalk resulting from the overlap of the signal from adjacent tracks. These areas were subtracted when integrating the total intensity of each track.

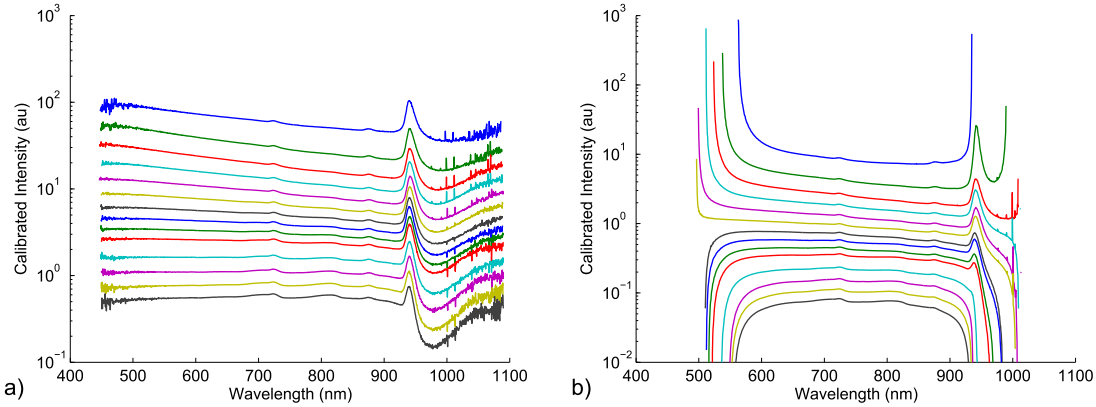

FIG. 8. Algorithm comparison. The spatially resolved spectra after correction for spectrometer transmission and detector response. Each line corresponds to a different source-detector distance on the probe surface. (a) The spectrum after processing using the algorithm described in this article. (b) The spectrum after processing with a very basic algorithm that uses straight line track boundaries and does not correct for crosstalk.

Gaussian function, Eq. (1). The model used to smooth the data was chosen by examining the coefficient of determination (R^2 value) as data in a large training set were fit with various models. The two-term Gaussian model produced a better fit to the observed data than a simpler one-term Gaussian. The "x" value in Eq. (1) is the pixel number, while parameters a_1 through c_2 are free parameters varied to produce the best fit to the observed data. The final track boundaries produced by this algorithm at each wavelength are shown in Fig. 6,

$$a_1 e^{-\left(\frac{x-b_1}{c_1}\right)^2} + a_2 e^{-\left(\frac{x-b_2}{c_2}\right)^2}. \quad (1)$$

Despite the attempt to minimize crosstalk through the physical arrangement of the fibre outputs across the CCD, crosstalk was still present in the data. This can be observed in the plot of Fig. 5, in which the base signal level between each adjacent track depends on the tracks' intensity. The amount of crosstalk in each track was estimated by finding the line connecting the data at both boundaries of each track, as illustrated in Fig. 7. Final reflectance values were obtained by integrating across each track and subtracting the crosstalk. Applying this method at each wavelength collected by the spectrometer provided a final spectrum for each distance on the fibre optic probe head.

III. RESULTS

A comparison between the image processing algorithm described here and a basic approach that uses straight lines for track boundaries was performed. A liquid phantom containing a lipid emulsion (Intralipid 20%, Fresenius Kabi AG, Bad Homburg, Germany) diluted to 0.65% was measured, and the images were processed and corrected for wavelength-dependent spectrometer transmission and detector response. The final spatially resolved spectra using each method are shown in Fig. 8. The data show a clear difference in results, especially at the outer ends of the spectrum. In fact, the algorithm extends the spectral range of the system since when using the basic algorithm (straight line boundaries, no crosstalk), the data for some of the tracks are unusable below 575 nm and above 925 nm.

IV. CONCLUSION

A technique for recovering spatially resolved spectra from diffuse reflectance images collected with an imaging spectrometer and CCD has been presented. This image processing routine automatically detects track edges on the raw CCD images and corrects for distortion introduced by the equipment. Crosstalk due to overlap of distinct spatially resolved signals is estimated and subtracted from the data. The spectra produced by this algorithm can be used with a steady state version of the Monte Carlo fitting routine described by Kienle and Patterson[19] to determine the optical properties of turbid media.

ACKNOWLEDGMENTS

This project is supported in part by the Natural Science and Engineering Research Council of Canada (Grant No. 365065) and Ontario Centres of Excellence (Grant No. 51860). Qiyin Fang holds the Canada Research Chair in Biophotonics.

[1]G. Vane, R. O. Green, T. G. Chrien, H. T. Enmark, E. G. Hansen, and W. M. Porter, Remote Sens. Environ. **44**, 127 (1993).
[2]M. C. De Sanctis, A. Coradini, E. Ammannito, G. Filacchione, M. T. Capria, S. Fonte, G. Magni, A. Barbis, A. Bini, M. Dami, I. Ficai-Veltroni, and G. Preti, Space Sci. Rev. **163**, 329 (2011).
[3]L. Gao, R. T. Kester, N. Hagen, and T. S. Tkaczyk, Opt. Express **18**, 14330 (2010).
[4]Z. Nie, R. An, J. E. Hayward, T. J. Farrell, and Q. Fang, J. Biomed. Opt. **18**, 096001 (2013).
[5]J. Pekar and M. S. Patterson, Med. Laser Appl. **25**, 147 (2010).
[6]A. Garcia-Uribe, E. B. Smith, J. Zou, M. Duvic, V. Prieto, and L. V. Wang, J. Biomed. Opt. **16**, 020501 (2011).
[7]A. Douplik, S. Zanati, G. Saiko, C. Streutker, M. Loshchenov, D. Adler, S. Cho, D. Chen, M. Cirocco, N. Marcon, J. Fengler, and B. C. Wilson, J. Biophotonics **7**, 304 (2014).
[8]H.-W. Wang, J.-K. Jiang, C.-H. Lin, J.-K. Lin, G.-J. Huang, and J.-S. Yu, Opt. Express **17**, 2805 (2009).
[9]A. E. Karsten, A. Singh, P. A. Karsten, and M. W. H. Braun, Lasers Med. Sci. **28**, 437 (2013).
[10]S. Nickell, M. Hermann, M. Essenpreis, T. J. Farrell, U. Kramer, and M. S. Patterson, Phys. Med. Biol. **45**, 2873 (2000).
[11]Z. Qian, S. Victor, Y. Gu, C. Giller, and H. Liu, Opt. Express **11**, 1844 (2003).

[12]G. M. Palmer, C. Zhu, T. M. Breslin, F. Xu, K. W. Gilchrist, and N. Ramanujam, IEEE Trans. Biomed. Eng. **50**, 1233 (2003).
[13]C. Zhu, G. M. Palmer, T. M. Breslin, J. Harter, and N. Ramanujam, Lasers Surg. Med. **38**, 714 (2006).
[14]J. R. Mourant, O. C. Marina, T. M. Hebert, G. Kaur, and H. O. Smith, J. Biomed. Opt. **19**, 37004 (2014).
[15]P. A. Valdes, A. Kim, F. Leblond, O. M. Conde, B. T. Harris, K. D. Paulsen, B. C. Wilson, and D. W. Roberts, J. Biomed. Opt. **16**, 116007 (2011).
[16]M. Gurfinkel, T. Pan, and E. M. Sevick-Muraca, J. Biomed. Opt. **9**, 1336 (2004).
[17]T. Svensson, J. Swartling, P. Taroni, A. Torricelli, P. Lindblom, C. Ingvar, and S. Andersson-Engels, Phys. Med. Biol. **50**, 2559 (2005).
[18]D. E. Hyde, T. J. Farrell, M. S. Patterson, and B. C. Wilson, Phys. Med. Biol. **46**, 369 (2001).
[19]A. Kienle and M. S. Patterson, Phys. Med. Biol. **41**, 2221 (1996).